Available online at www.sciencedirect.com

ScienceDirect

Journal of Magnesium and Alloys 8 (2020) 819–831

www.elsevier.com/locate/jma

Full Length Article

Kinetic modeling of high-temperature oxidation of pure Mg

Sa Ma[a], Fangzhou Xing[a], Na Ta[b], Lijun Zhang[a,*]

[a] *State Key Laboratory of Powder Metallurgy, Central South University, Changsha, Hunan 410083, P.R. China*
[b] *Max-Planck-Institut für Eisenforschung GmbH, Max-Planck-Straße 1, 40237, Düsseldorf, Germany*

Received 14 June 2019; received in revised form 24 December 2019; accepted 26 December 2019
Available online 2 June 2020

Abstract

A variety of experimental tracer diffusivities of Mg and O in magnesium oxide available in the literature were first assessed. Atomic mobilities including bulk and short-circuit diffusion of Mg and O were then obtained by means of the CALPHAD (Calculation of Phase Diagram) approach. Afterwards, the diffusion-controlled kinetic model of oxidation in a gas-MgO-Mg environment was developed based on the moving boundary model and Fick's law, coupling with the modified thermodynamic description of MgO. A mathematical expression for parabolic rate constant k_p of the oxide scale was derived for magnesia and correlated with the thermodynamic and diffusion kinetic information. The evaluated k_p results were in line with the experimental data. Finally, the oxidation process of pure magnesium at 673 K was model-predicted, and the predicted evolution of the oxide thicknesses agreed very well with the experimental data. It was indicated that the grain boundaries diffusion of magnesium cations predominated the high temperature oxidation process.

Keywords: MgO; Diffusion; Oxidation; Atomic mobility; CALPHAD; Wagner's model.

1. Introduction

Magnesium alloys possess excellent properties including low density, high specific strength and rigidity, good damping and cutting performance, great degradation behavior and biocompatibility, and thus serve as the key materials for realizing the lightweight of automobiles and biomedical applications [1-4]. However, the corrosion behavior limits the practical applications of magnesium alloys [5-7]. In order to improve the serviceability of magnesium alloys, it is crucial to study the oxidation of pure magnesium and even magnesium alloys, which will be helpful for comprehensive understanding of their oxidation mechanisms.

So far, there have been several experimental measurements of the oxidation process of pure magnesium [8-12]. However, it is very difficult to describe the oxidation behaviors over the wider temperature range through purely experimental measurements due to their relatively high time/money cost. Under this situation, some underlying modeling/numerical simulation techniques are highly needed to describe the oxidation process. In actual, the oxidation process of metals is a really complex one, involving the chemical reactions between metal and oxygen, as well as diffusion of cations and anions in oxides [13]. Considering the fact that the rate of chemical reactions depends on the diffusion of ions, the overall oxidation rate is mainly controlled by the mass transport through oxides. The general Wagner's model [14] provides an understanding of mass transport processes occurring within a growing oxide scale, thereby leading to a capacity to predict the effect on the changes of the oxidation rate along with the temperature. In the Wagner's model [14], the complex process, including the evolution of microstructures due to diffusion of ions, grain growth, defect annihilation, spallation, etc., was simplified, and the parabolic equation was derived by considering only the diffusion-controlled process. It should be noted that the parabolic rate constant in Wagner's model should generally

* Corresponding author.
E-mail addresses: lijun.zhang@csu.edu.cn, xueyun168@gmail.com (L. Zhang).

https://doi.org/10.1016/j.jma.2019.12.005

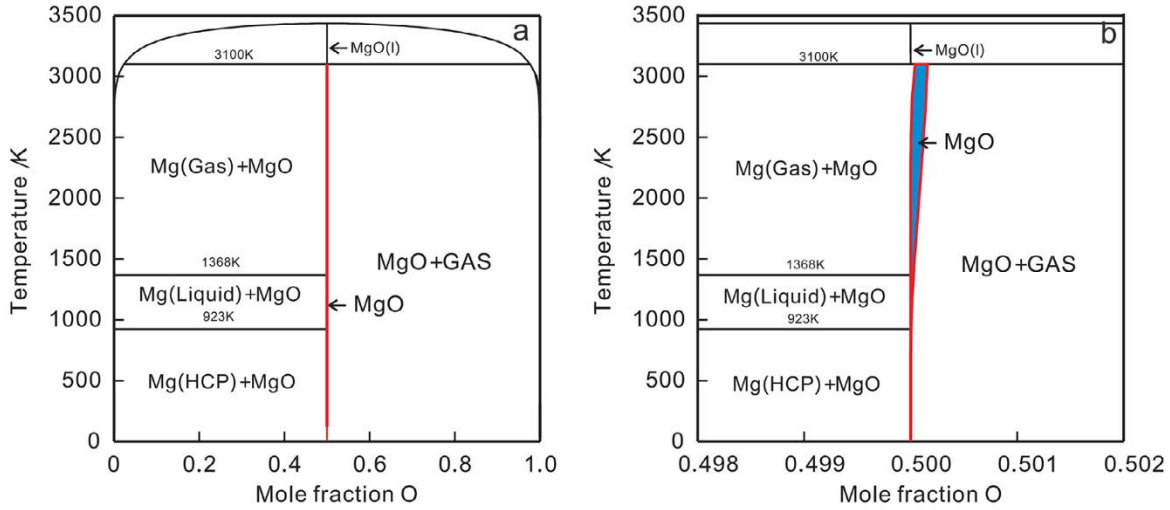

Fig. 1. (Color online) Calculated phase diagram of binary Mg-O system: (a) over the entire composition range; (b) in the vicinity of MgO compound, according to the thermodynamic descriptions originally from Hallstedt [16] together with the modified thermodynamic descriptions for MgO in this work.

depend on both thermodynamic and kinetic parameters, including oxygen activity and bulk diffusion coefficient. Very recently, Xing et al. [15] derived an equation for parabolic oxidation rate constant of Ni accounting for various diffusivities within the Wagner's framework. However, in Ref. [15], the empirical degree of defect ionization and vacancy concentration were introduced to replace the thermodynamic factor, which is not a general treatment for different metals/alloys. Thus, there is a need to correlate the parabolic rate constant with the general thermodynamic and kinetic information.

Up to now, only one set of thermodynamic descriptions [16] for the Mg-O binary system exist in the literature, while no relevant kinetic descriptions have been reported. The Diffusion-Controlled Transformation (DICTRA) software package, operating under the Calculation of PHAse Diagram (CALPHAD) framework, has been widely employed to establish the atomic mobility databases for different materials, from which various diffusivities of composition and temperature dependence can be predicted together with the reliable thermodynamic databases. During the past several years, DICTRA has been employed to develop the atomic mobility descriptions of the oxides for different metals, including pure Fe [17,18], Cr [19] and Al [20], as well as some complex oxides $LaCoO_{3-\delta}$ [21].

Consequently, the oxidation process of pure Mg at high temperatures is chosen as the target in the present work. The major objectives are: (*i*) to perform critical review of all the experimental tracer diffusivities of Mg and O in MgO in the literature, and obtain the self-consistent atomic mobility descriptions of O and Mg in MgO; (*ii*) to derive a mathematical expression for growth rate constant k_p of oxide scale by fully considering diffusion and thermodynamics in metal and oxygen ions in the framework of the Wagner's theory; and (*iii*) to predict the growth process of magnesium oxide during oxidation of pure magnesium, and clarify the oxidation mechanism of pure magnesium.

2. Literature review on various diffusivities in MgO

The diffusion behavior of magnesium cations in MgO has been extensively studied during the past years [22-29], and different types of diffusion coefficients of ions in Mg-O system are critically reviewed in the following and concisely summarized in Table 1.

The self-diffusivities of magnesium cations in MgO single crystals over the temperature range of 1400∼1600°C were first measured in 1957 by Lindner and Parfitt [22], who used the isotope exchange technology with the isotope ^{28}Mg. In their experiments, the impurities in magnesia were ignored, thus the magnesia was regarded as ideal crystals and the diffusion was intrinsic. They found that the activation energy of magnesium diffusion at low temperatures (<1400°C) was lower than that at higher temperature (>1400°C). After that, several further investigations on diffusion of magnesium in pure MgO single crystals were reported by Harding et al. [23,24] and Wuensch et al. [25]. Harding et al. [24] compared their experiment data with those by Lindner and Parfitt [22] and found that self-diffusion of magnesium in MgO is sensitive to the impurities and easily affected by short circuit diffusion at low temperatures. Wuensch et al. [25] employed ^{26}Mg rather than ^{28}Mg to measure the self-diffusion coefficients in an argon atmosphere. The experimental data measured by Harding et al. [23,24] are thus different from those by Lindner and Parfitt [22]. Moreover, the initial materials in the study of Wuensch et al. [25] contained even more impurities than those used by Lindner et al. [22], resulting in the inaccurate experimental self-diffusivities by Wuensch et al. [25].

In the aspect of short circuit diffusion of magnesium ions in MgO, Sakaguchi et al. [27] utilized ^{26}Mg to measure the diffusion coefficients of magnesium in single-crystal MgO, taking both bulk and dislocation diffusion into consideration. Orman et al. [28] measured the grain boundary diffusion coefficients of magnesium in polycrystal MgO at 2273 K.

Table 1
Summary of all the experimental diffusivities of Mg and O in MgO available in the literature

Diffusivity	Temperature/K	Tracer	Methods[a]	Reference	Materials and preparation[b]		Note[c]
$D_{Mg\text{-}bulk}$	1702∼1889	^{28}Mg	Sectioning	[22]	SC, 99.99%	Company	√
	1400∼2025	^{28}Mg	Sectioning	[23]	SC, 99.94%	Company	√
	1530∼2615	^{28}Mg	Sectioning	[24]	SC, 99.94%	Company	√
	1273∼2673	^{26}Mg	MS	[25]	SC, 99.80%	Company	√
	1121∼1238	-	-	[26]	SC, 99.96%	Company	√
	973∼1573	^{26}Mg	SIMS	[27]	SC, 99.96%	Company	√
$D_{Mg\text{-}gb}$	2273	^{25}Mg	IM	[28]	PC, 99.98%	Periclase	●
	1000∼2250	-	MD	[29]	PC, Ideal	Shell model	○
$D_{Mg\text{-}dis}$	973∼1273	^{26}Mg	SIMS	[27]	SC, 99.96%	Company	√
$D_{Mg\text{-}eff}$	1371∼1573	^{26}Mg	SIMS	[27]	SC, 99.96%	Company	●
$D_{O\text{-}bulk}$	1573∼2023	^{18}O	IE	[30]	SC, 99.92%	Periclase	√
	1367∼1667	^{18}O	IE	[32]	PC, 99.68%	Pyrolysis	√
	1273∼1773	^{18}O	IE	[33]	SC, 99.68%	Pyrolysis	√
	1573∼2023	^{18}O	IE	[34]	SC, 99.96%	Commercial	√
	1573∼2023	^{18}O	IE	[34]	SC, 99.98%	ORNL	√
	1673	^{18}O	SIMS	[35]	SC, 99.98%	ORNL	√
	1580∼1820	^{18}O	IE, PA	[36]	SC, 99.98%	ORNL	√
	1473∼1773	^{18}O	SIMS	[37]	SC, 99.98%	ORNL	√
	1473∼2373	^{18}O	SIMS	[38]	SC, HP	MBE	√
	1573∼1773	^{18}O	SIMS	[39]	BC, HP	CVT	√
	1273∼1923	^{18}O	SIMS	[40]	SC, HP	CVT	√
$D_{O\text{-}gb}$	1900∼2010	^{18}O	IE, PA	[31]	BC, 99.87%	-	√
	1320∼1700	^{18}O	SIMS	[32]	PC, 99.68%	Pyrolysis	√
	1400∼1728	^{18}O	-	[33]	PC, 99.68%	Pyrolysis	√
	1473∼1773	^{18}O	SIMS	[37]	PC, 99.99%	ORNL	√
	1573∼1773	^{18}O	SIMS	[39]	BC, HP	CVT	√
	2273	^{18}O	IM	[28]	PC, 99.98%	Periclase	√
	1000∼2250	-	MD	[29]	PC, Ideal	Shell model	○
$D_{O\text{-}dis}$	1473∼1773	^{18}O	SIMS	[37]	SC, 99.99%	ORNL	√

[a] SIMS: secondary ion mass spectroscopy, MS: mass spectrometer analysis, IM: ion microprobe, MD: molecular dynamics, IE: isotope exchange technology, PA: proton activation analysis.
[b] SC: single crystal, BC: bicrystal, PC: polycrystal, HP: high purity. ORNL: Oak Ridge National Laboratory; MBE: molecular beam epitaxy; CVT: chemical vapor transport.
[c] The sign represents whether the data are adopted in the present assessment. √: adopted for assessment, ○: not adopted during the assessment of mobilities but employed for comparing with the calculated results, ●: not adopted.

However, their experiments were under the condition of high pressure from 15 to 25 GPa. Recently, the molecular dynamic simulations were carried out by Landuzzi et al. [29] and the grain boundary diffusion coefficients of Mg and O in MgO were also evaluated.

Up to now, there have been many studies on diffusion coefficients of oxygen in MgO available in the literature [28-40]. In 1960, Oishi and Kingery [30] first measured the self-diffusion coefficients of oxygen anions in single-crystal MgO, and their measured self-diffusion coefficients of oxygen are smaller than those of the magnesium cations by two orders of magnitudes. However, their samples comprise a small amount of impurities. In 1971, the grain boundary diffusion coefficients of oxygen in MgO with bicrystals were measured by Mckenzie et al. [31] by means of Fisher's model [41]. Their results indicated that grain boundary diffusion would dominate predominantly the mass transport property in polycrystalline MgO at low temperatures. After that, the self-diffusion coefficients of oxygen were determined by Hashimoto et al. [32] in polycrystalline MgO by isotope exchange technology and they concluded that the diffusion of oxygen along the grain boundaries are relatively faster than the bulk diffusion of oxygen. One year later, Shirasaki and Hama [33] reported that the self-diffusivities of oxygen in loosely-sintered and well-sintered polycrystalline MgO, following the same approach by Hashimoto et al. [32]. Thereafter, Oishi et al. [34] measured two groups of the oxygen diffusivities in 1983, and the obvious differences between diffusion mechanisms at different temperatures were observed. They claimed that diffusion was impurity-insensitive at high temperatures while structure-sensitive at low temperatures, i.e., that the existence of dislocations and subgrains could increase the diffusion coefficients, which is actually in line with the diffusion mechanism of magnesium in MgO. In the same year, Henriksen et al. [35] determined the diffusivities of oxygen in pure, doped and deformed samples at 1673 K by means of the secondary-ion mass spectrometer (SIMS) method, and explained that the rate of oxygen diffusion in deformed materials was about fourfold larger than that in undeformed samples. Meanwhile, Reddy and Cooper [36] measured the diffusion coefficients of oxygen in MgO in the temperature range of 1580 to 1820 K. Then, ^{18}O was used as a tracer element in single crystals, deformed single crystals and polycrystals of MgO, and thus bulk, dislocation and grain boundary diffusion

coefficients of ^{18}O were measured by means of SIMS method by Dolhert [37]. In 1994, Yang and Flynn [38] measured the diffusivities of oxygen anions using high-purity magnesium oxides produced by molecular beam epitaxy (MBE), which is smaller than others by about two orders of magnitude. After that, Liberatore and Wuensch [39] measured the diffusion coefficients of oxygen in bulk and grain boundaries by using MgO bicrystals with high purity prepared by chemical vapor transport (CVT) and concluded that the enhancement of diffusivities was more conspicuous along grain boundaries with higher energy. In 2002, Yoo et al. [40] evaluated the prefactor and activation energy of oxygen diffusion coefficients in larger range of temperature and the smaller standard deviations were observed. In 2015, the molecular dynamic simulations were also applied by Landuzzi et al. [29] to evaluate the grain boundary diffusion coefficients of oxygen that deviate largely from the experimental data [32,33,37,39].

3. Model descriptions

3.1. Thermodynamic model

The Mg-O phase diagram was reported by Wriedt [42] in 1987. It was pointed out by Wriedt [42] that MgO is not an ideal stoichiometric compound but with a very narrow homogeneity range. However, the specific homogeneity range has never been reported so far. In 1993, Hallstedt [16] assessed the thermodynamic description of the Mg-O system by means of CALPHAD approach. Hallstedt [16] firstly took the solubility of oxygen in liquid magnesia into account, while the solubility of oxygen was not considered in the solid magnesia, and MgO was thus treated as an ideal stoichiometric compound. In addition, the site occupations of ions in lattice were regular, so the formula unit of solid magnesia with two sublattices was written as $(Mg^{2+})_1(O^{2-})_1$, where the first sublattice denotes the octahedral interstices and the second one was occupied by oxygen anions in a face-centered cubic (fcc) lattice. It should be noted that the vacancies were not considered in the formula unit, and thus the MgO phase was treated as a rigid stoichiometric phase.

Although the homogeneity range of MgO is too narrow to be measured accurately, it should not be neglected in the study of diffusion kinetics. The similar treatment in our previous studies on binary Co-Si [43] and Al-O systems [20] is also applied to the present Mg-O system, i.e., that very tiny homogeneity range can be introduced in MgO by modifying its thermodynamic descriptions but keeping the deviation of the invariant reaction temperatures within 2 K. Based on the thermodynamic description by Hallstedt [16], the new sublattice model $(Mg^{2+}, Mg^{3+}, Va)_1(O^{2-})_1$ was employed for MgO by introducing the magnesium cations with high valence to maintain the electro-neutrality. As a result, the molar Gibbs energy of MgO phase can be written as:

$$G_m = y^I_{Mg^{2+}}\,{}^0G_{Mg^{2+}:O^{2-}} + y^I_{Mg^{3+}}\,{}^0G_{Mg^{3+}:O^{2-}} + y^I_{Va}\,{}^0G_{Va:O^{2-}} + RT\left(y^I_{Mg^{2+}}\ln y^I_{Mg^{2+}} + y^I_{Mg^{3+}}\ln y^I_{Mg^{3+}} + y^I_{Va}\ln y^I_{Va}\right) + G^{ex} \quad (1)$$

where y^i_X is site fraction of X in the i sublattice, ${}^0G_{A:B}$ is the mole Gibbs energy of the end member of compound, and G^{ex} the excess Gibbs energy. In this work, ${}^0G_{Mg^{3+}:O^{2-}} = {}^0G_{Mg^{2+}:O^{2-}} + 70000$, ${}^0G_{Va:O^{2-}} = 0$ and $G^{ex} = 0$ were set, while the other parameter ${}^0G_{Mg^{2+}:O^{2-}}$ was kept as the reported values in Hallstedt's original work [16].

Based on thermodynamic descriptions originally from Hallstedt [16] together with those for MgO modified in this work, the phase diagram of binary Mg-O system was calculated, as presented in Fig. 1. As can be seen in the enlarged part of the Mg-O phase diagram, a very narrow homogeneity range exists in the MgO compound now. With the derived thermodynamic descriptions for MgO in Eq. (1), the site fractions of vacancy at the stoichiometric composition of MgO under the condition of $P(O_2)$=0.21 atm was computed and plotted in Fig. 2(a). Moreover, the corresponding thermodynamic factor and chemical potential of O in MgO as a function of O compositions at 673 K were also calculated and shown in Fig. 2(b). As can be seen in Fig. 2, the site fraction of vacancy increases as the temperature increases, while the chemical potential profile indicates that the direction of driving force is consistent with the concentration gradient. Moreover, as the mole fraction of oxygen is close to 0.5, the thermodynamic factor will approach to the infinity. Under this circumvent, the so-called average thermodynamic factor as proposed in [43] is also introduced here. The detailed discussion can be referred to the Appendix.

3.2. Diffusion kinetic model

The oxidation rate of magnesium at high temperatures is controlled by diffusion [44], which is driven by the gradient of chemical potential. Based on the Ågren's theory, the flux of the ions in the lattice-fixed reference frame is given as [17]

$$J_{Mg} = -\left(y^I_{Mg^{2+}}y^I_{Va}M_{Mg^{2+}Va} + y^I_{Mg^{3+}}y^I_{Va}M_{Mg^{3+}Va}\right)\frac{1}{V_0}\frac{\partial\mu_{Mg}}{\partial z} \quad (2)$$

where μ_i is the chemical potential, V_0 the volume per mole of anion sites. M_{iVa} is atomic mobility of component i jumping from one site to a neighboring site and has the form: $M_{iVa}=M_0\exp(-Q/RT)$, in which M_0 is the frequency factor, which is the function of vibrational frequency (ν), jump distance (δ) and temperature (T) *via* $M_0=\delta^2\nu/RT$, while Q is the activation energy. Here, by assuming that atomic mobilities of magnesium cations in the first sublattice have the relationship $M_{Mg^{2+}Va}=M_{Mg^{3+}Va}=M_{MgVa}$, Eq. (2) can be simplified as

$$J_{Mg} = -y^I_{Mg}y^I_{Va}M_{MgVa}\frac{1}{V_0}\frac{\partial\mu_{Mg}}{\partial z} \quad (3)$$

According to Ref. [17], one can obtain the expression for the tracer diffusion coefficients D^*_{Mg}, which is given by

$$D^*_{Mg} = y^I_{Va}RTM_{MgVa} \quad (4)$$

Compared with Einstein's equation: $D^*=RTM$, the atomic mobility of magnesium in MgO can be inferred

$$M_{Mg} = y^I_{Va}M_{MgVa} \quad (5)$$

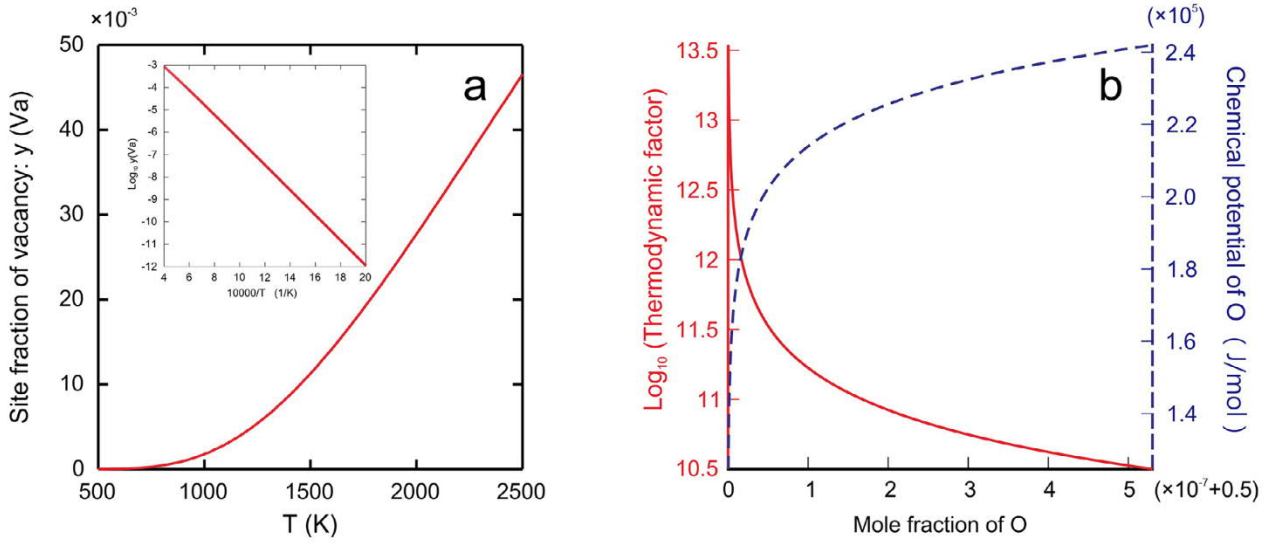

Fig. 2. (Color online) Calculated (a) site fractions of vacancy at the stoichiometric composition of MgO under the condition of $P(O_2)$=0.21 atm; (b) thermodynamic factors (red solid line) and chemical potentials (blue dash line) of O in MgO as function of O composition at 673 K, based on the presently obtained thermodynamic descriptions for MgO with slight modifications of the original parameters from Hallstedt [16].

As mentioned above, the ions in MgO diffuse according to the vacancy mechanism. Although the second sublattice is fully occupied by oxygen anions in the thermodynamic model above, there are a few sites for vacancies, of which the contribution is too small to be considered in the thermodynamic model. Supposing that the site fractions of species in the second sublattice are y^{II}_{Va} and y^{II}_{O}, the flux of the tracer O* along z axis in a lattice-fixed frame of reference can also be expressed in the similar way,

$$J_O = -y^{II}_{Va} M_{OVa} RT \frac{\partial c_O}{\partial z} \tag{6}$$

which yields:

$$D^*_O = y^{II}_{Va} RT M_{OVa} \tag{7}$$

Then, the atomic mobility of oxygen has the form:

$$M_O = y^{II}_{Va} M_{OVa} \tag{8}$$

It should be noted that there are several types of diffusivities besides the bulk diffusivity in normal lattice. As a matter of fact, there are various defects in real crystals, like dislocations and grain boundaries in polycrystals, which can largely enhance the diffusion velocity through reducing the activation energy. Considering the influence caused by defects, it is necessary to use effective diffusion coefficients to replace the bulk diffusivity in the present work. To quantitatively analyze the diffusion behavior in real polycrystals, the model proposed by Hart [45] and Harrison [46] was utilized to describe the effective diffusion coefficients in this work [47]. The same frequency factor with bulk diffusion but a redistributed coefficient F_{red} for activation energy was introduced in the circuit diffusion compared with the bulk atomic mobility. Then, the atomic mobilities along dislocation and grain boundaries can be expressed as

$$M^{DIS} = M_0^{bulk} \exp\left(\frac{-F_{redDIS} Q^{bulk}}{RT}\right)$$

$$M^{GB} = M_0^{bulk} \exp\left(\frac{-F_{redGB} Q^{bulk}}{RT}\right) \tag{9}$$

where the value of redistributed coefficient in the equation is generally less than 1 for the circuit diffusion. F_{red} is in relation to the energy of the defects, including Burger's vector and thickness of grain boundaries, where Burgers vector's square represents the energy of a dislocation, and the grain boundary thickness, to some extent, represents the energy of a grain boundary. Besides, the effective diffusion coefficients are connected to the quantity of the defects relating to the key factors, namely, the dislocation density and grain size. Thus, the effective mobility and diffusion coefficients can be expressed as [45,46]

$$wM_{eff} = \frac{3\delta}{d} M^{GB} + \rho b^2 M^{DIS} + \left(1 - \frac{3\delta}{d} - \rho b^2\right) M^{bulk}$$

$$D_{eff} = \frac{3\delta}{d} D^{GB} + \rho b^2 D^{DIS} + \left(1 - \frac{3\delta}{d} - \rho b^2\right) D^{bulk} \tag{10}$$

here δ denotes the average thickness of grain boundaries, d average grain size which depends on the temperature and time, ρ dislocation density and b Burgers vector. D^{bulk}, D^{DIS}, D^{GB} and D_{eff} are the tracer diffusion coefficients in bulk, dislocation and grain boundary and the effective tracer diffusion coefficients, respectively.

3.3. Oxidation kinetic model

The diffusion-controlled oxidation process obeys the parabolic law. According to the Wagner's theory [14]:

$$X^2 = k_p t \tag{11}$$

where X represents the oxide thickness (unit: m), k_p oxide growth rate constant (unit: m^2/s) and t time (unit: s). Based on Eq. (11), the key to evaluate the thickness of oxides as a

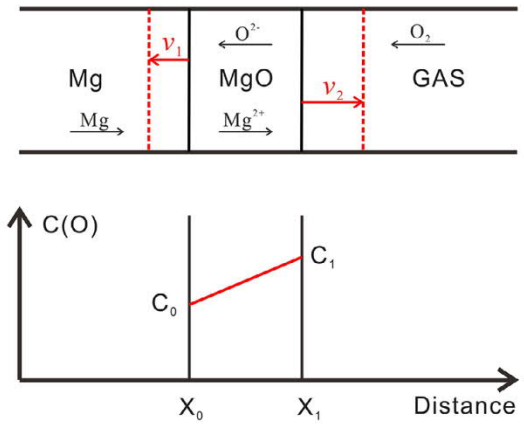

Fig. 3. (Color online) Schematic diagram for the oxidation process of pure Mg as well as growth process of MgO.

function of time lies in the reasonable value of k_p, which is determined by both thermodynamics (driving force) and kinetics (diffusion coefficients). In fact, the reliable thermodynamic and kinetic information needed for k_p can be provided by the CALPHAD-type thermodynamic and kinetic descriptions. The derivation of the mathematical expression for k_p is described in the following.

The oxidation rate can be determined by the moving rate of interfaces, including both oxide/metal and oxide/gas interfaces. The inward diffusion of oxygen ions results in an internal migrating interface towards pure Mg, while the outward diffusion of magnesium ions can cause an external migrating interface towards gas. The schematic diagram is shown in Fig. 3. Based on the moving boundary model [20], the moving rate of boundary has the form:

$$\frac{v}{V_m^{\alpha}}x_k^{\alpha} - \frac{v}{V_m^{\beta}}x_k^{\beta} = J_k^{\alpha} - J_k^{\beta} \tag{12}$$

where v denotes moving rate of interface, V_m^i the molar volume of i (i=α, β) phase and J_k^i the diffusion flux of component k in i phase, which can be expressed by Fick's first law:

$$J_k = -D_k\frac{\partial c_k}{\partial x} \tag{13}$$

Here, D_k denotes chemical diffusion coefficient of component k. D_k can be related to the tracer diffusion coefficient D_k^* and thermodynamic factor [16] via the following equation:

$$D_k = D_k^*\frac{n_k}{RT}\frac{\partial \mu_k}{\partial n_k},\ (k = \mathrm{Mg},\ \mathrm{O}) \tag{14}$$

Since thermodynamic factor for a nearly stoichiometric compound is infinity, the average thermodynamic factor defined as [43] is introduced and the detail discussion is listed in the Appendix. The combination of Eqs. (12)–(14), and may determine the moving rates of two interfaces of oxide phase, respectively. Therefore, the values of k_p can be determined by the sum of moving rates of interfaces in both sides and finally simplified into:

$$k_p = \frac{\Delta\mu_O}{RT}\left(D_{Mg}^* + D_O^*\right) = \Delta\mu_O\left(M_{Mg} + M_O\right) \tag{15}$$

where $\Delta\mu_O$ denotes the difference of chemical potential of oxygen in magnesium oxide. According to the local equilibrium hypothesis, the identical components in the two phases have the same chemical potentials at interface. Thus, the chemical potentials of oxygen at two interfaces equal to those of gas and Mg (hcp) phase respectively. Moreover, since magnesium oxide owns a very narrow homogeneity range, i.e., that MgO is nearly a stoichiometric compound, the variation of chemical potential of oxygen can be expressed by:

$$\Delta\mu_O = G_m^{Mg} + G_m^{O_2} - 2G_m^{MgO} \tag{16}$$

Here, G_m^i denotes the molar Gibbs energy of i phase. The detail derivation process of Eq. (17) can also be referred to the Appendix. Based on Eqs. and , one can easily evaluate the oxidation rate constant k_p according to the available thermodynamic and kinetic descriptions, from which the evaluation of the thickness of oxides as a function of time can be easily performed instead of the complex numerical simulations.

4. Results and discussion

4.1. Bulk diffusion in MgO

The atomic mobilities for bulk diffusion in MgO were assessed on the basis of various experimental diffusivities in the bulk MgO available in the literature by means of a non-linear least-squares optimization scheme incorporated in the PARROT module of the DICTRA software package. The experimental tracer diffusivities of Mg in MgO in Refs. [22-27] as displayed in Fig. 4(a) were used to assess the atomic mobility parameters of Mg. On the contrary, as shown in Fig. 4(b), the experimental data of O [30,32-40] have a larger scatter because the purity of samples reported in the literature are not identical, which is one of the relating key factors of diffusion coefficients. The impurity contents may change the quantity of vacancies, ions interaction and substructures, thereby, influencing the tracer diffusion coefficients. The samples studied in the Refs. [30,32,33] with the highest impurity correspond to the highest diffusion coefficients in Fig. 4 (b). Conversely, the samples in Ref. [38] with the highest purity possess the lowest diffusion coefficients. Moreover, the samples with similar purity have the diffusion coefficients close with each other. Therefore, the experimental data from Ref. [38] were accepted to evaluate the atomic mobility descriptions for O in MgO. The other data in Fig. 4(b) are considered as the results of the combined contributions of the bulk and short circuit diffusion, which will be discussed in *Section 4.3*. The evaluated atomic mobility parameters are expressed as Eq. (17):

$$M_{MgVa}^{bulk} = 1.0481\times10^{-6}\exp\left(\frac{-233634.8}{RT}\right)\mathrm{m}^2/\mathrm{s}$$
$$M_{OVa}^{bulk} = 5.9341\times10^{-7}\exp\left(\frac{-504943.3}{RT}\right)\mathrm{m}^2/\mathrm{s} \tag{17}$$

The calculated bulk diffusion coefficients of the magnesium cations and oxygen anions as a function of inverse absolute temperature under different oxygen partial pressures and

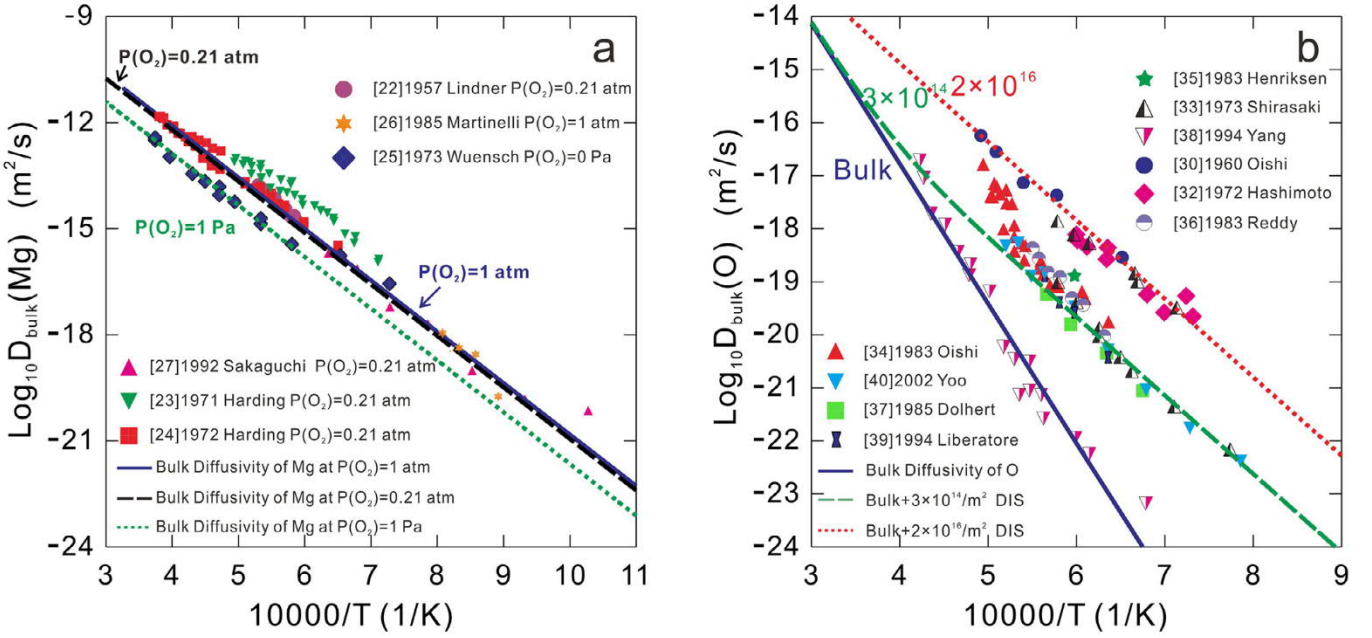

Fig. 4. (Color online) Calculated bulk diffusion coefficients of (a) Mg and (b) O in MgO as a function of inverse temperature and oxygen partial pressure, compared with the experimental data [22-27,30,32-40].

temperatures are shown in Fig. 4, compared with the experimental data [22-27]. It should be noted that the partial oxygen pressure determines the vacancy concentration in MgO, which affects the diffusion coefficients according to Eq. (4) and (7). As can be seen in Fig. 4 (a), the calculated temperature-dependent bulk diffusion coefficients of magnesium increase slightly as the partial oxygen pressure increases and agree very well with most of the experimental data [22,24-27]. It should be noted that the experimental data in Ref. [23] deviate from the calculated results because the impurities exist in the tracer solution, as explained in Ref. [24]. As can be seem in Fig. 4(b), the calculated bulk diffusion coefficients of oxygen also accord with the experimental data in Ref. [38].

4.2. Short-circuit diffusion in MgO

In practice, most materials are polycrystal, and thus a large amount of defects such as grain boundaries and dislocations coexist. As mentioned in Section 3.2, the jumping rates of atoms along the short-circuit paths such as grain boundaries and dislocations are much higher than that in the lattice. Therefore, the contributions of both grain boundaries and dislocations to diffusion should be taken into account. On the basis of Eq. (9), the mobilities along the short-circuit paths were evaluated by the same method declared above.

The experimental diffusivities of Mg along the dislocations reported in Ref. [27], shown in Fig. 5(a), were employed to assess the atomic mobility parameters. Moreover, the experimental data in Ref. [37], as shown in Fig 5(b), were used to assess the atomic mobility parameters of O along the dislocations, the obtained atomic mobility parameters along the dislocations are presented as follows:

$$M^{\mathrm{DIS}}_{\mathrm{MgVa}} = 1.0481 \times 10^{-6} \exp\left(\frac{-130387.6}{RT}\right) \mathrm{m}^2/\mathrm{s}$$

$$M^{\mathrm{DIS}}_{\mathrm{OVa}} = 5.9341 \times 10^{-7} \exp\left(\frac{-282749.7}{RT}\right) \mathrm{m}^2/\mathrm{s} \qquad (18)$$

As shown in Fig. 5, both calculated diffusivities of Mg and O conform to the experimental data in Ref. [27] and Ref. [37] respectively. Comparing the mobility along the dislocations with that in the bulk, the redistributed coefficients of activation energy along the dislocations can be calculated as $F^{\mathrm{Mg}}_{\mathrm{redDIS}} = 0.558$, $F^{\mathrm{O}}_{\mathrm{redDIS}} = 0.560$.

Besides the dislocation diffusion coefficients, the grain boundary diffusion coefficients of Mg and O are also studied, and the results are displayed in Fig. 6. For the oxygen anions, there are several groups of experimental data on the grain boundary diffusion coefficients available in the literature, including the data from the experimental measurements [31-33,37,39] and the molecular dynamics simulations [29]. The molecular simulation results scatter much larger over several magnitudes than the experimental data, and thus were not used in this work. Moreover, the scattering between different sets of experiments [31-33,37,39] for the grain boundary diffusion coefficients of O is about two magnitudes. It is quite normal because the high-angle grain boundaries have higher energy than the low-angle grain boundaries along which the diffusivities are lower [39]. In order to balance the influences from different categories of grain boundary, the average grain boundary diffusion coefficients of O were used by fitting to all the experimental data [31-33,37,39], and the results can be seen in Fig. 6(b).

Due to lack of data on magnesium diffusion along grain boundaries (except for one piece of information from

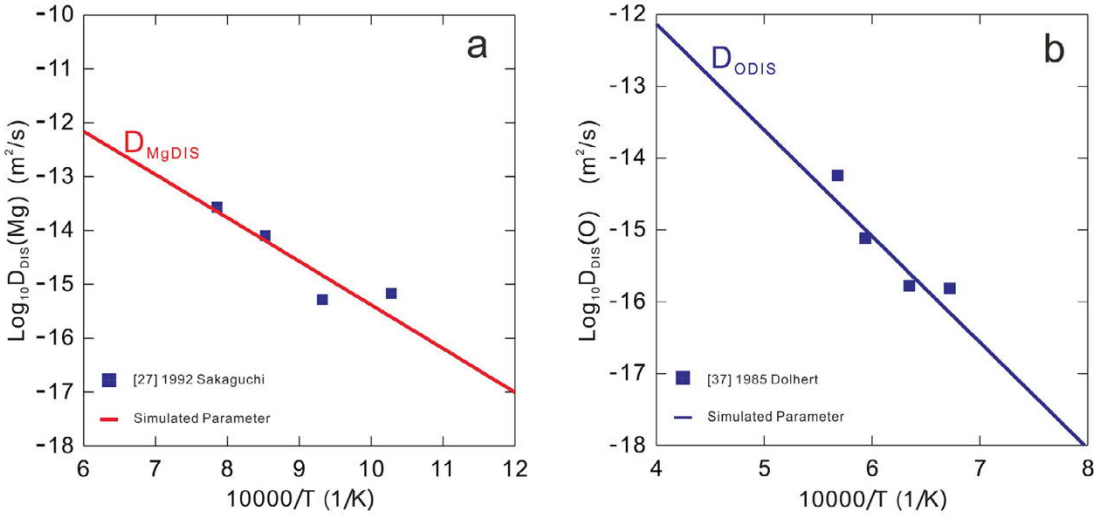

Fig. 5. (Color online) Calculated dislocation diffusivities of (a) Mg and (b) O in MgO as a function of inverse temperature, compared with the experimental data [27,37].

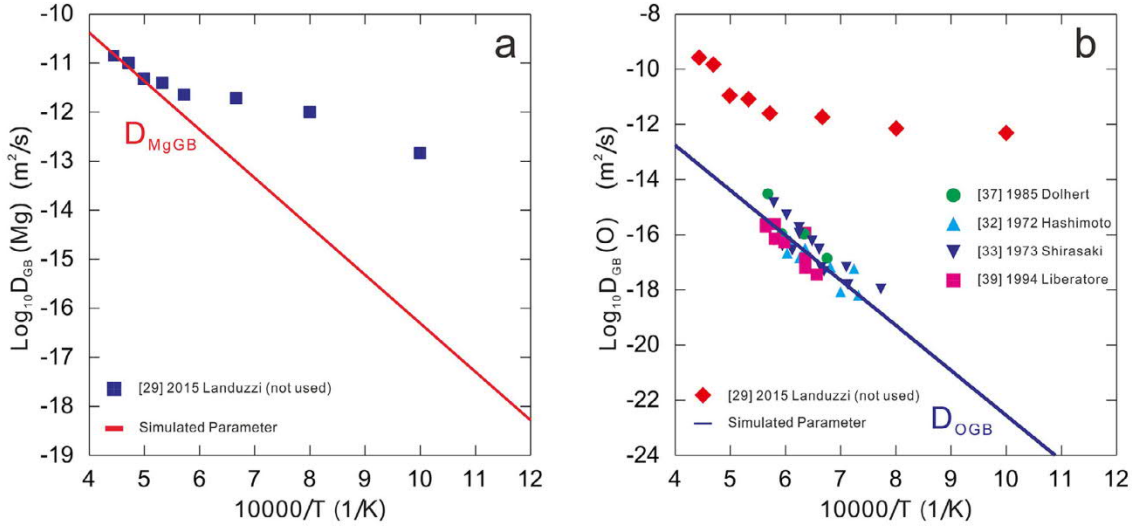

Fig. 6. (Color online) Calculated grain boundary diffusivities of (a) Mg and (b) O in MgO as a function of inverse temperature, compared with the experimental/theoretical data [29,31-33,37,39].

molecular dynamics simulations [29] which cannot be accepted in the present work), no assessment for magnesium mobility for the grain boundary diffusion was performed here. As discussed above, the redistributed coefficients of Mg and O along dislocations are nearly the same. Thus, it seems reasonable to assume that the grain boundary diffusion coefficients of Mg and O also have the same redistributed coefficient, as adopted in this work to predict the grain boundary diffusion coefficients of Mg in MgO. The predicted grain boundary diffusion coefficients of Mg in MgO as a function of inverse temperature are presented in Fig. 6(a).

The finally obtained atomic mobility parameters of Mg and O diffusion along grain boundaries are given as

$$M^{GB}_{MgVa} = 1.0481 \times 10^{-6} \exp\left(\frac{-144601.9}{RT}\right) m^2/s$$

$$M^{GB}_{OVa} = 5.9341 \times 10^{-7} \exp\left(\frac{-312520.9}{RT}\right) m^2/s \quad (19)$$

Here, Eq. (19) represents the average grain boundary mobilities. As shown in Fig. 6(a), the predicted grain boundary diffusion coefficients agree with the molecular dynamics results from Landuzzi et al. [29] at temperatures higher than 2000 K. When the temperature is the lower than 2000 K, the noticeable differences between the two values exist, and become larger and larger as the temperature decreases. As can be seen in Fig. 6(b), the agreement between calculated results and the experimental data seems to be good. Moreover, the mobility for diffusion of O along the high-angle grain boundaries is higher by about ten times than the average value, which is however higher than the mobility for diffusion of O along the low-angle grain boundaries by around ten times. The

redistributed coefficients of grain boundary diffusion coefficients of Mg and O can be evaluated as $F^{Mg}_{redGB} = F^{O}_{redGB} = 0.619$.

4.3. Effective diffusion in MgO

With Eq. (10), the effective diffusion coefficients can be evaluated based on the obtained atomic mobility parameters for diffusion along the bulk and short-circuit paths.

The factors influencing the diffusion along dislocation include dislocation density and burgers vector. As reported in the literature [27,37,48], the dislocation density is insensitive to the change of temperature. The values of dislocation density in MgO are in the range of 1×10^{13} /m^2 $\sim$ 1×10^{15} /m^2 [27,37]. In this work, the typical value ρ=1×10^{14} /m^2 was adopted. Besides, the burgers vector of main dislocations is $\frac{a}{2} < 110 >$ considering that MgO is with the face-centered cubic structure [49-51]. Based on the lattice parameters available in the literature, the length of burgers vector can be calculated as 0.297 nm [50]. Therefore, the value of ρb^2 in Eq. (10) is calculated in the order of 10^{-5}. One can obviously see that the contribution of diffusion along the dislocation to the effective diffusion is small and thus may be neglected.

As mentioned in *Section 4.1*, all the experimental data except the data from Ref. [38] were not used to evaluate the atomic mobility parameters because the purity of samples was not satisfactory. That is because the impurities in those samples may largely enhance the diffusion coefficients. To some extent, the content of impurities can be viewed as the dislocation since both of them can serve as the fast path for diffusion. As presented in Fig. 4(b), the influences of different dislocation densities on the bulk diffusion are compared with the experimental data with different impurities, and the results show a good agreement with the experimental data.

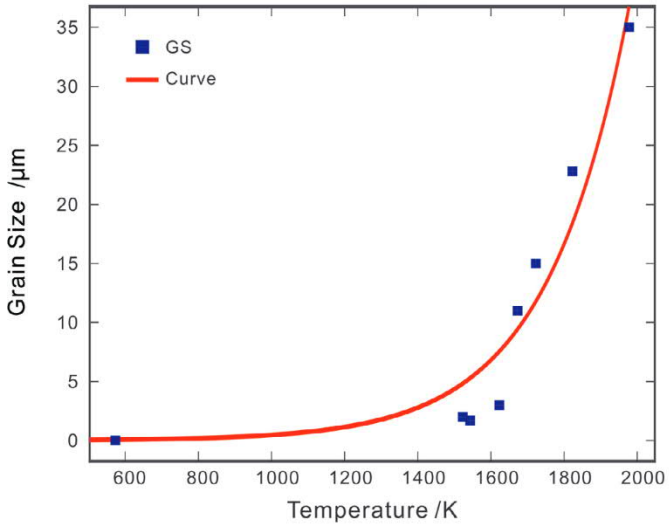

Fig. 7. (Color online) Calculated average grain size of MgO as a function of temperature, compared with the experimental data [29,31-33,37,48,52,53].

As for the grain boundary diffusion, the influence factors include the thickness of grain boundary and the average grain size. As reported in the literature, the thickness can be viewed as a constant for simplification, and thus the typical value δ=1 nm [28,29,31,39] was adopted here. Moreover, as the temperature increases, the grains may coarse, resulting in the decrease of interface energy. Therefore, the average grain size should be a function of temperature, i.e., d=$A\exp(BT)$, where d denotes the average grain size, while A and B are the undefined constants. As shown in Fig. 7, the temperature-dependent average grain sizes can be obtained by fitting to the experimental data [29,31-33,37,48,52,53] using a least-square method:

$$d = 5.399 \times 10^{-9} \exp(0.004463T) \quad (20)$$

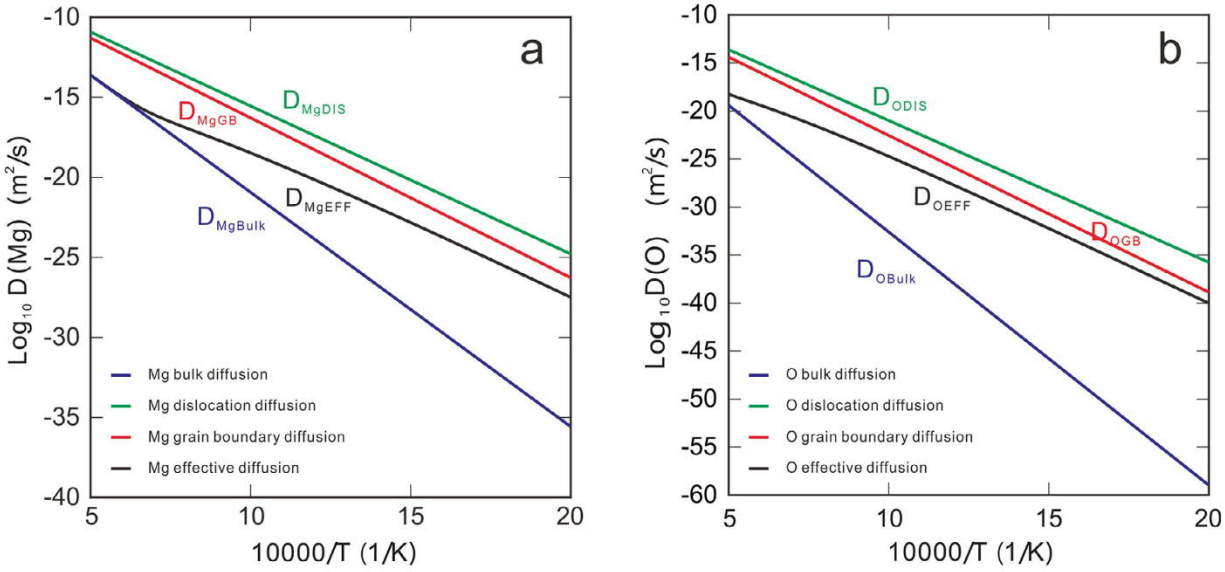

Fig. 8. (Color online) Model-predicted effective diffusion coefficients of (a) Mg and (b) O as a function of inverse temperature, compared with the bulk and short-circuit diffusion coefficients.

where d is the average grain size in the dimension of m, T temperature in K.

Based on the obtained atomic mobility parameters and the values for factors ρ, b, d, δ, the effective diffusion coefficients can be evaluated, and displayed in Fig. 8. As can be seen in Fig. 8, at higher temperatures, the effective diffusion coefficients are close to the bulk diffusion coefficients but show large scattering at lower temperature conversely. It can be explained by the different grain sizes existing at different temperatures. As the temperature decreases, the grains become smaller and there are more grain boundaries to enhance the diffusion of ions. By contrast, at high temperatures, the large grains eliminate the effect of grain boundaries on diffusion. Therefore, the contributions of short-circuit paths to diffusion can be ignored at higher temperatures but turn to be more and more essential as the temperature decreases. For instance, as shown in Fig. 8(b), the extrapolated value of D_{Obulk} at 500 K is close to $\sim 10^{-60}$ m^2/s, while those of D_{OGB} and D_{ODIS} are in the range of $10^{-40} \sim 10^{-35}$ m^2/s. It should be noted that the reliability of the obtained effective diffusion coefficients at lower temperatures needs further confirmation because it is very difficult to measure the grains with several nanometers accurately. Moreover, by comparing Fig .8 (a) with Fig. 8(b), the effective diffusion coefficients of O are much lower than those of magnesium cations. Base on Eq. (15) , it can be concluded that the high-temperature oxidation process of pure Mg is predominantly controlled by diffusion of the magnesium cations.

4.4. Oxide growth rate constant k_p and prediction of oxidation process of pure Mg

Based on the kinetic model of oxidation in *Section 3.3*, the growth rate constant of oxides k_p can be evaluated based on Eqs. (15) and (16) by the thermodynamic and kinetic descriptions obtained in this work. In order to truly reveal the oxidation mechanism, different sets of k_p values were calculated by considering different types of diffusion coefficients (i.e., bulk, grain boundary and/or effective diffusion coefficients). The calculated results and the experimental growth rate constants are shown in Fig. 9, where the experimental k_ps were calculated based on Eq. (11) together with the experimental thickness in Refs. [8-12], while the model-predicted values of k_p were calculated by the bulk diffusion coefficients (black line), grain boundary diffusion coefficients (blue line) and effective diffusion coefficients with different grain boundary angles (red, green, orange lines), respectively. Based on

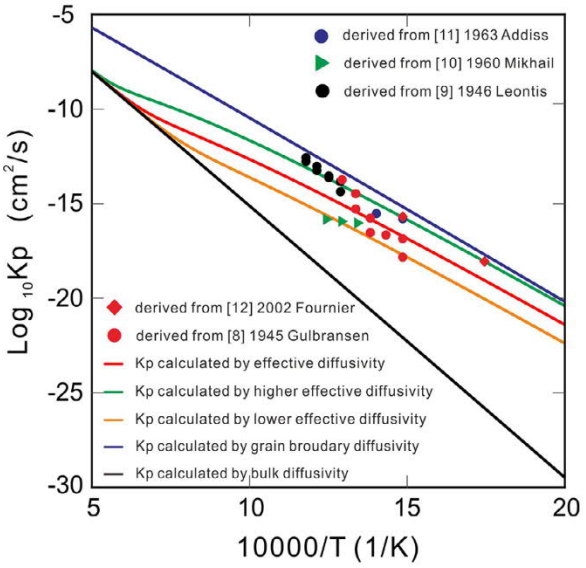

Fig. 9. (Color online) Logarithmic values of growth rate constant of oxide k_p as a function of inverse temperature from 500 K to 2000 K, compared with the experimental data [8-12].

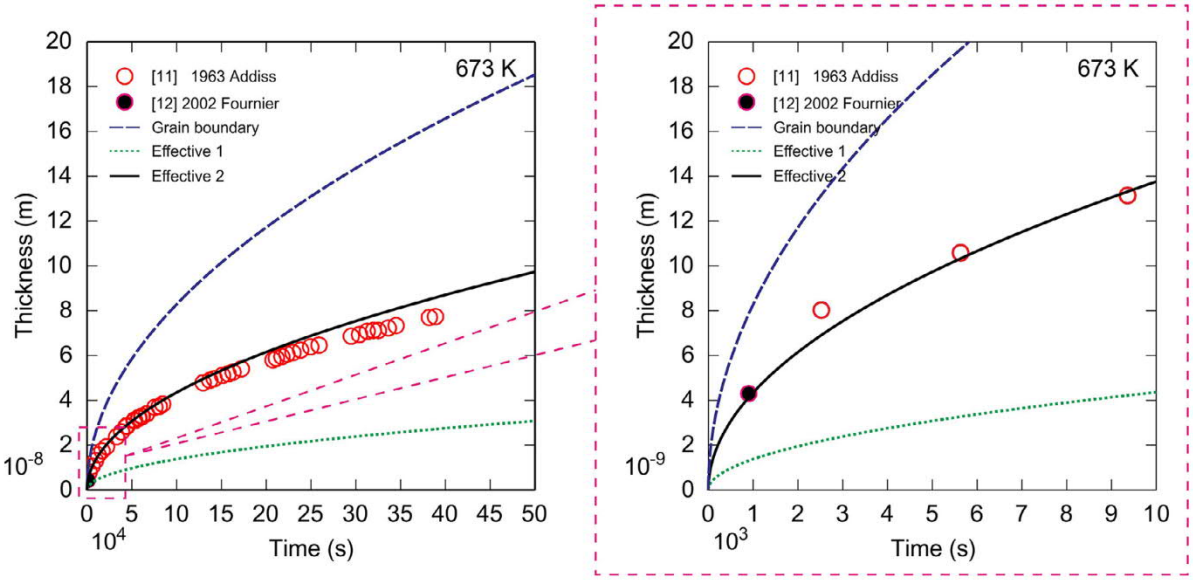

Fig. 10. (Color online) Model-predicted evolution of thickness of MgO oxide at 673K and $P(O_2)$=0.21 atm using different sets of diffusivities, compared with the experimental data [11,12].

Eq. (11), the oxide thickness as a function of time can be directly predicted by the evaluated k_p. The model-predicted thickness of MgO at $P(O_2)$=0.21 atm and 673K is presented in Fig. 10. It can be found that the model-predicted thickness according to the effective diffusivities with the high-angle grain boundaries can reproduce all the experimental data perfectly, which indicates the high-angle grain boundaries exist predominantly in the MgO polycrystals at 673 K.

From Fig. 9 and Fig. 10, one can conclude (*i*) that the calculated results based on the effective diffusivities reproduce the experimental data satisfactorily, which illustrates the reliability of the presently evaluated atomic mobility descriptions for Mg and O in MgO; (*ii*) that the grain boundaries can largely enhance the oxidation rate, especially at low temperatures; and (*iii*) that the grain boundaries with high angles can enhance the diffusion coefficients more effectively than those with low angles.

Though the predicted k_p values and thicknesses of MgO during oxidation are consistent with the experimental data, one should bear in mind that the naturally formed oxide film on Mg is quite diverse and depends on various factors. For example, the contributions of defects like grain boundary and dislocation were included in Eq. (10), but some empirical or typical parameters of defects were used due to lack of sufficient experimental data on i.e., the thickness of grain boundary, and the dislocation density. Therefore, in order to perform the quantitative modeling of the real oxidation process in different metals/alloys, the accurate description of microstructure evolution during the oxidation process should be a prior, which will be the topic for next paper.

5. Conclusions

- Atomic mobility descriptions for Mg and O in MgO were first obtained by means of CALPHAD approach based on various diffusion coefficients critically reviewed from the literature, together with the reported thermodynamic descriptions. Both bulk diffusion and short-circuit diffusion were taken in account. Different diffusivities evaluated according to the obtained atomic mobilities agree well with most of the experimental data.
- A mathematical expression for growth rate constant k_p of oxide scale by fully considering diffusion and thermodynamics in metal and oxygen ions was proposed in the framework of the Wagner's theory. The growth rate constant k_p of magnesium oxide was predicted by the obtained atomic mobility descriptions, and the predicted k_ps show a good agreement with the experimental data.
- The growth of magnesium oxide as a function of time at 673 K was simulated based on the Wagner's model. The simulated results with high-angle grain boundaries reproduced the experiments satisfactorily. Furthermore, the mechanism of magnesium oxidation over a wide range of temperature was discussed. The results indicate that grain boundary diffusion of magnesium cations predominated during the high temperature oxidation process.

Acknowledgements

The financial support from the National Key Research and Development Program of China (Grant No. 2016YFB0301101), the Hunan Provincial Science and Technology Program of China (Grant No. 2017RS3002)-Huxiang Youth Talent Plan, and the Youth Talent Project of Innovation-driven Plan at Central South University (Grant No. 2282019SYLB026) is acknowledged. Sa Ma acknowledges the financial support by the Fundamental Research Funds for the Central Universities of Central South University (Grant No. 2019zzts485). The authors thank Prof. Bengt Hallstedt at Aachen University, Germany for kindly providing thermodynamic database of Mg-O system.

Appendix. Derivation of oxide growth rate constant k_p

The modified formula unit of solid magnesium oxide phase is given with two sublattices as:$(Mg, Va)_1(O)_1$, where the valences of ions are neglected. Nevertheless, to ensure the diffusion of oxygen in the second sublattice based on vacancy diffusion mechanism, the formula unit can be rewritten as $(Mg, Va)_1(O,Va)_1$. As reported in Ref. [13], the chemical diffusion coefficients of magnesium and oxygen ions in magnesium oxide can be expressed by:

$$D_{Mg} = D^*_{Mg}\frac{n_{Mg}}{RT}\frac{\partial \mu_{Mg}}{\partial n_{Mg}}, \quad D_O = D^*_O\frac{n_O}{RT}\frac{\partial \mu_O}{\partial n_O} \tag{A1}$$

Here, n_i (i=Mg, O) represents the number of species i per mole first or second sublattice sites, which can be regarded as one during calculation since the fraction of vacancy is close to zero. Because the mole fraction x_i has a relationship with $n_i(x_i = n_i/(n_{Mg}+n_O))$, the chemical diffusion coefficient of O in Eq. (A1) can thus be deduced as:

$$\begin{aligned} D_O &= D^*_O\frac{n_O}{RT}\frac{\partial \mu_O}{\partial x_O}\frac{\partial x_O}{\partial n_O} = \frac{D^*_O}{RT}\frac{n_O n_{Mg}}{(n_{Mg}+n_O)^2}\frac{\partial \mu_O}{\partial x_O} \\ &= \frac{D^*_O}{4RT}\frac{\partial \mu_O}{\partial x_O} = \frac{D^*_O}{4RT}\phi \end{aligned} \tag{A2}$$

where ϕ is thermodynamic factor which can be determined from thermodynamic description. And the chemical diffusivity of Mg has the same form. Using the Gibbs-Duhem relationship, and x_{Mg}=x_O=0.5, one can express the chemical diffusivity of Mg as:

$$D_{Mg} = \frac{D^*_{Mg}}{4RT}\frac{\partial \mu_{Mg}}{\partial x_{Mg}} = \frac{D^*_{Mg}}{4RT}\frac{\partial \mu_O}{\partial x_O} = \frac{D^*_{Mg}}{4RT}\phi \tag{A3}$$

In the stoichiometric compound, the average thermodynamic factor ϕ_{ave}[41] needs to be introduced to replace ϕ for evaluation of the diffusion coefficients:

$$\phi_{ave} = \int_{x_1}^{x_2}\frac{\partial \mu_O}{\partial x_O}dx_O = \frac{\mu_2-\mu_1}{x_2-x_1} = \frac{\Delta\mu_O}{\Delta x_O} \tag{A4}$$

where x_1 and x_2 respectively denote minimum and maximum of mole fraction of oxygen in MgO, μ_1 and μ_2 are chemical potentials. According to Eq. (16), the chemical potential difference $\Delta\mu_O$ could be calculated.

As is mentioned in Section 3.3, the distance between the two interfaces of MgO phase related to the interface moving rate, is the thickness of oxide film. Based on Eq. (12), interface moving rates could be deduced by chemical diffusion flux. It should be noted that the mole fraction of O in magnesium and the mole fraction of Mg in gas are approximated to be zero, resulting in zero flux of component O and Mg in pure magnesium phase and gas phase, respectively. Moreover, the mole fractions of magnesium and oxygen in MgO are both 0.5. Therefore, combined with the Fick's first law, the absolute values of interface moving rates could be derived as:

$$|v_1| = 2V_m D_O \left|\frac{\partial c_O}{\partial X}\right|, \qquad |v_2| = 2V_m D_{Mg} \left|\frac{\partial c_{Mg}}{\partial X}\right| \tag{A5}$$

where v_1 and v_2 respectively denote moving rate of metal/oxide interface and oxide/gas interface, V_m the volume occupied by per mole ions (sum of magnesium and oxygen ions). V_m is considered as independent of composition. It is reasonable to assume that the concentration profiles within MgO phase region is linear at any time as magnesium oxide has very narrow homogeneity range. Thus, the growth rate of magnesium oxide could be determined by interface moving rates:

$$\frac{\partial X}{\partial t} = |v_1| + |v_2| = \frac{2V_m}{X}\left(D_O|\Delta c_O| + D_{Mg}|\Delta c_{Mg}|\right) = \frac{2}{X}\left(D_O|\Delta x_O| + D_{Mg}|\Delta x_{Mg}|\right) \tag{A6}$$

where Δx_O and Δx_{Mg} respectively represent mole fraction difference of O and Mg, and $\Delta x_O = \Delta x_{Mg}$. Combine Eq. (11) with the solution of Eq. (A6), growth rate constant of oxide k_p is derived as:

$$k_p = 4|\Delta x_O|\left(D_O + D_{Mg}\right) = \frac{\Delta\mu}{RT}\left(D^*_{Mg} + D^*_O\right) \tag{A7}$$

References

[1] J. Zhang, S. Liu, R. Wu, L. Hou, M. Zhang, Recent developments in high-strength Mg-RE-based alloys: Focusing on Mg-Gd and Mg-Y systems, J. Magnesium Alloys 6 (3) (2018) 277–291.

[2] V.K. Bommala, M.G. Krishna, C.T. Rao, Magnesium matrix composites for biomedical applications: A review, J. Magnesium Alloys 7 (1) (2019) 72–79.

[3] T. Cheng, Y. Tang, L.J. Zhang, Update of thermodynamic descriptions of the binary Al-Sn and ternary Mg-Al-Sn systems, CALPHAD: Comput. Coupling Phase Diagrams Thermochem. 64 (2019) 354–363.

[4] H.J. Si, Y.X. Jiang, Y. Tang, L.J. Zhang, Stable and metastable phase equilibria in binary Mg-Gd system: A comprehensive understanding aided by CALPHAD modeling, J. Magnesium Alloys 7 (2019) 501–513.

[5] Q.Y. Tan, A. Atrens, N. Mo, M.X. Zhang, Oxidation of magnesium alloys at elevated temperatures in air: A review, Corros. Sci. 112 (2016) 734–759.

[6] A. Bahmani, S. Arthanari, K.S. Shin, Corrosion behavior of Mg–Mn–Ca alloy: Influences of Al, Sn and Zn, J. Magnesium Alloys 7 (1) (2019) 38–46.

[7] X. Zhang, J. Dai, R. Zhang, Z. Ba, N. Birbilis, Corrosion behavior of Mg–3Gd–1Zn–0.4Zr alloy with and without stacking faults, J. Magnesium Alloys 7 (2) (2019) 240–248.

[8] E.A. Gulbransen, The oxidation and evaporation of magnesium at temperatures from 400° to 500°C, Trans. Electrochem. Soc. 87 (1) (1945) 589–599.

[9] T. Leontis, F. Rhines, Rates of high temperature oxidation of magnesium and magnesium alloys, Trans. Amer. Inst. Min. (matall.) Engrs. 166 (1946) 265–294.

[10] R.S. Mikhail, V.K. Gouda, Rate of oxidation of magnesium metal in dry oxygen, J. Appl. Chem. 10 (9) (1960) 384–388.

[11] J.R.R. Addiss, Oxidation of magnesium single crystals and evaporated films, Acta Metall. 11 (2) (1963) 129–135.

[12] V. Fournier, P. Marcus, I. Olefjord, Oxidation of magnesium, Surf. Interface Anal. 34 (1) (2002) 494–497.

[13] T.-L. Cheng, Y.-H. Wen, J.A. Hawk, Diffuse-interface modeling and multiscale-relay simulation of metal oxidation kinetics - with revisit on wagner's theory, J. Phys. Chem. C 118 (2) (2014) 1269–1284.

[14] C. Wagner, Beitrag zur theorie des anlaufvorgangs, Z. Phys. Chem. 21 (1) (1933) 25–41.

[15] F.Z. Xing, N. Ta, J. Zhong, Y. Zhong, L.J. Zhang, Kinetic modeling of high-temperature oxidation of pure nickel, Solid State Ionics 341 (2019) 115018.

[16] B. Hallstedt, The magnesium-oxygen system. CALPHAD: Comput, Coupling Phase Diagrams Thermochem 17 (3) (1993) 281–286.

[17] S. Hallström, L. Höglund, J. Ågren, Modeling of iron diffusion in the iron oxides magnetite and hematite with variable stoichiometry, Acta Mater. 59 (1) (2011) 53–60.

[18] H. Larsson, T. Jonsson, R. Naraghi, Y. Gong, R.C. Reed, J. Ågren, Oxidation of iron at 600 °C - experiments and simulations, Mater. Corros. 68 (2) (2017) 133–142.

[19] S. Hallström, M. Halvarsson, L. Höglund, T. Jonsson, J. Ågren, High temperature oxidation of chromium: Kinetic modeling and microstructural investigation, Solid State Ionics 240 (2013) 41–50.

[20] N. Ta, L.J. Zhang, Q. Li, Z. Lu, Y. Lin, High-temperature oxidation of pure Al: Kinetic modeling supported by experimental characterization, Corros. Sci. 139 (2018) 355–369.

[21] N. Ta, M. Chen, L.J. Zhang, C. Chatzichristodoulou, W.M. Chen, P.V. Hendriksen, Y. Du, Numerical simulation of kinetic demixing and decomposition in a $LaCoO_3$-delta oxygen membrane under an oxygen potential gradient, J. Membr. Sci. 548 (2018) 526–539.

[22] R. Lindner, G.D. Parfitt, Diffusion of radioactive magnesium in magnesium oxide crystals, J. Chem. Phys. 26 (1) (1957) 182–185.

[23] B.C. Harding, D.M. Price, A.J. Mortlock, Cation self-diffusion in single crystal MgO, Philos. Mag. 23 (182) (1971) 399–408.

[24] B.C. Harding, D.M. Price, Cation self-diffusion in MgO up to 2350°C, Philos. Mag. 26 (1) (1972) 253–260.

[25] B.J. Wuensch, W.C. Steele, T. Vasilos, Cation self-diffusion in single-crystal MgO, J. Chem. Phys. 58 (12) (1973) 5258–5266.

[26] J.R. Martinelli, E. Sonder, R.A. Weeks, R.A. Zuhr, Measurement of cation diffusion in magnesium oxide by determining the $Mg^{18}O$ buildup produced by an electric field, Phys. Rev. B: Condens. Matter Mater. Phys. 32 (10) (1985) 6756–6763.

[27] I. Sakaguchi, H. Yurimoto, S. Sueno, Self-diffusion along dislocations in single-crystals MgO, Solid State Commun. 84 (9) (1992) 889–893.

[28] J.A. Van Orman, Y. Fei, E.H. Hauri, J. Wang, Diffusion in MgO at high pressures: Constraints on deformation mechanisms and chemical transport at the core-mantle boundary, Geophysical Res. Lett. 30 (2) (2003).

[29] F. Landuzzi, L. Pasquini, S. Giusepponi, M. Celino, A. Montone, P.L. Palla, F. Cleri, Molecular dynamics of ionic self-diffusion at an MgO grain boundary, J. Mater. Sci. 50 (6) (2015) 2502–2509.

[30] Y. Oishi, W.D. Kingery, Oxygen Diffusion in Periclase Crystals, J. Chem. Phys. 33 (3) (1960) 905–906.

[31] D.R. Mckenzie, A.W. Searcy, J.B. Holt, R.H. Condit, Oxygen grain-boundary Diffusion in MgO, J. Am. Ceram. Soc. 54 (4) (1971) 188–190.

[32] H. Hashimoto, M. Hama, S. Shirasaki, Preferential diffusion of oxygen along grain boundaries in polycrystalline MgO, J. Appl. Phys. 43 (11) (1972) 4828–4829.

[33] S. Shirasaki, M. Hama, Oxygen-diffusion characteristics of loosely-sintered polycrystalline MgO, Chem. Phys. Lett. 20 (4) (1973) 361–365.

[34] Y. Oishi, K. Ando, H. Kurokawa, Y. Hirsco, Oxygen self-diffusion in MgO single crystals, J. Am. Ceram. Soc. 66 (4) (1983) C-60-C-62.

[35] A.F. Henriksen, Y.-M. Chiang, W.D. Kingery, W.T. Petuskey, Enhanced oxygen diffusion at 1400°C in deformed single-crystal magnesium oxide, J. Am. Ceram. Soc. 66 (8) (1983) C-144-C-146.
[36] K. Reddy, A.R. Cooper, Oxygen diffusion in MgO and α-Fe_2O_3, J. Am. Ceram. Soc. 66 (9) (1983) 664–666.
[37] L.E. Dolhert, Oxygen diffusion in dislocations and grain boundaries in magnesium oxide Ph.D. thesis, Massachusetts Institute of Technology, Cambridge, MA, 1985.
[38] M.H. Yang, C.P. Flynn, Intrinsic diffusion properties of an oxide: MgO, Phys. Rev. Lett. 73 (13) (1994) 1809–1812.
[39] M. Liberatore, B.J. Wuensch, Oxygen self-diffusion in MgO grain boundaries, Mater. Res. Soc. Symp. Proc. 357 (1995) 389–393.
[40] H. Yoo, B.J. Wuensch, W.T. Petuskey, Oxygen self-diffusion in single-crystal MgO: secondary-ion mass spectrometric analysis with comparison of results from gas-solid and solid-solid exchange, Solid State Ionics 150 (3-4) (2002) 207–221.
[41] J.C. Fisher, Calculation of diffusion penetration curves for surface and grain boundary diffusion, J. Appl. Phys. 22 (1) (1951) 74–77.
[42] H. Wriedt, The Mg–O (magnesium-oxygen) system, Bulletin of Alloy Phase Diagrams 8 (3) (1987) 227–233.
[43] L.J. Zhang, Y. Du, Y. Ouyang, H. Xu, X.G. Lu, Y. Liu, Y. Kong, J. Wang, Atomic mobilities, diffusivities and simulation of diffusion growth in the Co–Si system, Acta Mater. 56 (15) (2008) 3940–3950.
[44] H. Zheng, S. Wu, H. Sheng, C. Liu, Y. Liu, F. Cao, Z. Zhou, X. Zhao, D. Zhao, J. Wang, Direct atomic-scale observation of layer-by-layer oxide growth during magnesium oxidation, Appl. Phys. Lett. 104 (14) (2014) 141906.
[45] E. Hart, On the role of dislocations in bulk diffusion, Acta Metall. 5 (10) (1957) 597.
[46] L. Harrison, Influence of dislocations on diffusion kinetics in solids with particular reference to the alkali halides, Trans. Faraday Soc. 57 (1961) 1191–1199.
[47] J.O. Andersson, J. Ågren, Models for numerical treatment of multicomponent diffusion in simple phases, J. Appl. Phys. 72 (4) (1992) 1350–1355.
[48] H. Yurimoto, H. Nagasawa, The analysis of dislocation pipe radius for diffusion, Mineral. J. 14 (5) (1989) 171–178.
[49] J. Narayan, J. Washburn, Self diffusion in magnesium oxide, Acta Metall. 21 (5) (1973) 533–538.
[50] Y. Moriyoshi, T. Ikegami, S.-I. Matsuda, Y. Bando, Y. Sekikawa, S.-I. Shirasaki, Formation of Subgrain Boundaries in Magnesium Oxide Single Crystals, Z. Phys. Chem. 118 (2) (1979) 187–195.
[51] S.C. Parker, N.H. De Leeuw, D.J. Harris, F.M. Higgins, P.M. Oliver, S.E. Redfern, G.W. Watson, Atomistic simulation of oxide dislocations and interfaces, Radiat Eff. Defects Solids 151 (1-4) (1999) 185–195.
[52] J.D. Hodge, R.S. Gordon, Grain growth and creep in polycrystalline magnesium oxide fabricated with and without a Lif additive, Ceramurg. Int. 4 (1) (1978) 17–20.
[53] T. Vasilos, J.B. Mitchell, R.M. Spriggs, Creep of Polycrystalline Magnesia, J. Am. Ceram. Soc. 47 (4) (2010) 203–204.